Japanese Journal of Radiology (2019) 37:579–589
https://doi.org/10.1007/s11604-019-00848-w

ORIGINAL ARTICLE

Comparison of magnetization transfer contrast of conventional and simultaneous multislice turbo spin echo acquisitions focusing on excitation time interval

Syo Murata[1] · Yasuhiko Tachibana[1,2] · Katsutoshi Murata[3] · Koji Kamagata[1] · Masaaki Hori[1] · Christina Andica[1] · Michimasa Suzuki[1] · Akihiko Wada[1] · Kanako Kumamaru[1] · Akifumi Hagiwara[1,4] · Ryusuke Irie[1,4] · Shuji Sato[1] · Nozomi Hamasaki[1] · Issei Fukunaga[1] · Haruyoshi Hoshito[1] · Shigeki Aoki[1]

Received: 9 January 2019 / Accepted: 14 June 2019 / Published online: 22 June 2019

Abstract

Purpose Image contrast differs between conventional multislice turbo spin echo (conventional TSE) and multiband turbo spin echo (SMS-TSE). Difference in time interval between excitations for adjacent slices (SETI) might cause this difference. This study aimed to evaluate the influence of SETI on MT effect for conventional TSE and compare conventional TSE with SMS-TSE in this respect.

Materials and methods Three different agar concentration phantoms were scanned with conventional TSE by adjusting SETI and TR. Signal change for different SETI was evaluated using Pearson's correlation analysis. SMS-TSE was acquired by changing TR similarly. Three human volunteers were scanned with similar settings to evaluate reproducibility of the phantom results in human brain.

Results In conventional TSE, shorter SETI induced larger signal reduction. Longer TR and higher agar concentration emphasized this characteristic. Significant linear correlation ($P < 0.05$) was found in the major cases. The SMS-TSE signal intensity in each TR and phantom was smaller than the assumable levels in conventional TSE when the slices were simultaneously excited. Similar characteristic was observed in human brain.

Conclusion Shorter SETI results in larger MT effect in conventional TSE. The contrast change in SMS-TSE was larger than the supposable level from simultaneous excitation, which needs consideration in clinics.

Keywords Multiple simultaneous slices · Magnetization transfer effect · Turbo spin echo sequence · Multiband imaging · Fast imaging

Introduction

Recently, a multiband technique that simultaneously excites multiple slices has been developed for high-speed imaging [1]. Its useful application in several fields has been reported, including diffusion-weighted imaging and perfusion-weighted imaging [2, 3]. Turbo spin echo (TSE) using this multiband technique (simultaneous multislice TSE: SMS-TSE) is another useful application of this technique, especially in scans for pediatric patients, because its shorter scan time contributes to a reduction in motion artifacts that is often problematic for children [4, 5]. However, the image contrasts obtained with conventional multislice TSE and SMS-TSE are empirically different, which might not be ignored for clinical usage. One of the major reasons for this difference might be the

Electronic supplementary material The online version of this article (https://doi.org/10.1007/s11604-019-00848-w) contains supplementary material, which is available to authorized users.

✉ Yasuhiko Tachibana
yaz.tachibana@radio.email.ne.jp

[1] Department of Radiology, Juntendo University, 2-1-1 Hongo, Bunkyo-ku, Tokyo 113-0033, Japan

[2] Applied MRI Research, Department of Molecular Imaging and Theranostics, NIRS, QST, Chiba, Japan

[3] Siemens Healthcare K.K., Tokyo, Japan

[4] Department of Radiology, Graduate School of Medicine, The University of Tokyo, Tokyo, Japan

difference in the strengths of the magnetization transfer (MT) effect. As a typical example of MT effect-related contrast change in *T*1-weighted imaging of human brain, the contrast between the basal ganglia and the surrounding white matter becomes larger when the MT effect generated by the imaging sequence is larger. Here, as the white matter contains more macromolecules (i.e., myelin) than the basal ganglia, the signal reduction due to the MT effect is larger in the white matter. Thus, the contrast between the two tissues will be emphasized more in the imaging sequence that causes stronger MT effect.

MT is a dipole-interaction-related energy transfer phenomenon that occurs as a result of the chemical exchange of protons between macromolecules and water molecules [6–10]. Generally, *T*2 of a macromolecule proton is extremely short (i.e., 1 ms or less); therefore, the signal from this proton cannot be directly acquired by clinical magnetic resonance imaging (MRI). This is because the echo time (TE) cannot be sufficiently shortened for this *T*2 range. However, since the magnetic saturation is transferred to the water (liquid) proton that has a longer *T*2 (i.e., 10 ms or more) through MT, the magnetization of a macromolecule proton can be indirectly observed as a signal loss of water protons. This phenomenon is called the MT effect. Since the bandwidth of the resonance frequency is narrow for a water proton and wide for a macromolecule proton, when an off-resonance radio-frequency (RF) pulse is applied to a field where water protons and macromolecule protons coexist, the signal of the water protons decreases owing to the saturation that first occurred in the macromolecules and was then transferred to the water protons. Some clinical scan sequences effectively utilize this phenomenon [11–14], but the changes in the image contrast derived from this effect become a problem in general multislice imaging [15, 16]. The mechanism of the MT effect in two-slice imaging (as a simple example of multislice imaging) is well explained by Henkeman et al. [17]. The mechanism can be summarized as follows. In this example, we defined the "first slice" as the slice where the magnetization of a macromolecular proton occurs by application of an RF pulse, and the "second slice" as the slice where the MT effect is observed as a reduction in the signal.

1. A slice-selective RF pulse for the first slice is applied. The water protons existing in the area of the first slice and the macromolecule protons existing in a wide area including the first- and second-slice areas are excited (saturated).
2. The saturation of macromolecular protons existing in the area of the second slice is transferred to nearby liquid protons within a very short time (i.e., MT), whereby some water protons of the second slice become saturated (partial saturation).
3. Longitudinal relaxation of the saturated water protons existing in the second-slice area occurs until the RF pulse is applied to the second slice. However, when the longitudinal relaxation of these protons is not complete—even at the time of when the RF pulse is applied to the second slice—the signal observed in the second slice decreases according to the degree of incompleteness.

In this example, it can be assumed that the strength of the MT effect, i.e., the magnitude of the signal reduction in the second slice, is influenced by the slice excitation time interval (SETI) between the excitation of the two slices. This is because the degree of longitudinal relaxation that occurs in step 3 might change when the SETI changes. This assumption has not been thoroughly discussed, most likely because the SETI is automatically determined in typical clinical MRI and cannot be changed. However, if the SETI has a strong influence on the MT effect, this might be the reason for the altered contrast observed in SMS-TSE. This is because, when simply focusing on the time interval between slice excitations, SMS-TSE is similar to a conventional multislice TSE scan with SETI being shortened to the limit, i.e., when assuming that SMS-TSE is a sequence where the SETI is shortened far below the typical range (even though there are some other differences between short SETI multislice TSE and SMS-TSE). Therefore, the aims of this study are: (1) to evaluate the influence of SETI on MT effect for conventional multislice TSE and, (2) to compare conventional multislice TSE with SMS-TSE in this respect.

Materials and methods

This study was approved by the local ethics review board of (blinded) and subjects' informed consent was obtained. In this study, three agar phantoms and one ultrapure water phantom were scanned with a 3-T MRI machine (MAGNETOM Skyra, Siemens Healthcare, Erlangen, Germany) equipped with a 64-channel head coil. As a continuous imaging protocol, several images were acquired to obtain the *T*1, *T*2, and magnetic transfer ratio (MTR) maps. Next, conventional multislice TSE with an adjusted-SETI length (adjusted-SETI TSE) was carried out, followed by SMS-TSE (prototype version). Then, the images were evaluated to assess the properties of the phantoms, the effect of SETI on the signal intensities and the differences between adjusted-SETI TSE and SMS-TSE. The details are described in the following sections.

Preparation and evaluation of the phantoms

Three agar phantoms with different agar concentrations and one ultrapure water phantom were prepared using ultrapure water and agar powder according to previous reports [18, 19]. Three agar phantoms were created by adding agar powder to boiled water and then sealing them in plastic cases. According to previous reports [11, 12, 18], these three phantoms had agar concentrations of 2, 4, and 8% so that the relaxation times of the agar phantoms were close to that of human tissues as much as possible. An ultrapure water phantom was created by sealing ultrapure water in the same plastic case. This process was carefully performed to ensure that the phantoms did not contain air bubbles, which was later confirmed by the images obtained in this study. Then, the three agar phantoms and one ultrapure water phantom were enclosed in a larger plastic case filled with ultrapure water to avoid susceptibility artifacts. The four phantoms were arranged inside the larger case so that they could be scanned simultaneously (Fig. 1). All of the scans were performed three times, and the images were averaged for assessment. To evaluate the properties of the phantoms, *T*1, *T*2, and MTR maps were obtained. The major imaging parameters are summarized in Table 1. *T*1 maps were calculated from the images obtained by the double flip angle (FA) gradient echo method using B1 correction of the turbo fast low-angle shot (turboFLASH) [20]. *T*2 maps were obtained from the images acquired by the multiecho spin echo method. The commercial software (Mapit, Siemens Healthcare, Erlangen, Germany) installed on the MR device was used for these calculations. The MTR was obtained by a method using a magnetization transfer contrast (MTC) pulse. The MTC pulse equipped in the MRI system (pulse shape = Gaussian, pulse duration = 9.984 ms, pulse off-resonance = 1200 Hz, FA = 500°) was used for this purpose. MTR maps were calculated from the acquired images as

$$\mathrm{MTR} = \left(\mathrm{MTC_{off}} - \mathrm{MTC_{on}}\right)/\mathrm{MTC_{off}}, \quad (1)$$

where $\mathrm{MTC_{on}}$ and $\mathrm{MTC_{off}}$ are the signal intensities acquired with and without an MTC pulse, respectively.

A circular region of interest (ROI) with a radius of 5 mm was set at the center of each phantom where the signal intensity seemed the most homogeneous. *T*1 maps were used to define the ROIs, which were copied and pasted to other metric maps. All of the ROI-based measurements were performed by copying and pasting these ROIs. The values of the pixels inside the ROIs were averaged in each ROI to obtain the *T*1, *T*2, and MTR values of each phantom [11, 12].

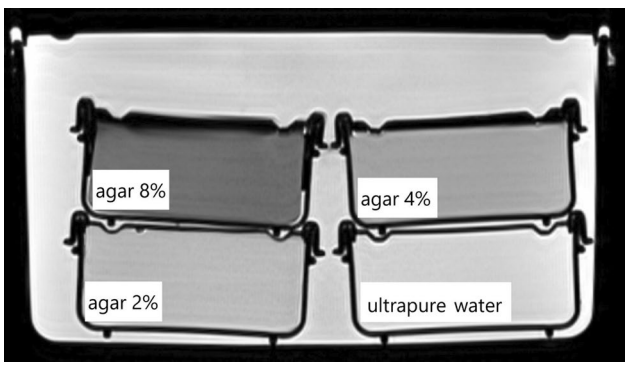

Fig. 1 Three agar phantoms with different agar concentrations (2, 4, and 8%) and an ultrapure water phantom were prepared for this study. Four plastic cases were used to seal these agar solutions and ultrapure water separately; then, they were enclosed in a larger plastic case filled with ultrapure water. The phantoms were arranged as shown to scan all of them simultaneously

Table 1 Imaging parameters for calculating the values of *T*1, *T*2, and the magnetization transfer ratio

	*T*1	*T*2	MTR
Imaging sequence	3D FLASH	2D spin echo	3D FLASH
Repetition time (ms)	15	1200	30
Echo time (ms)	1.83	9.9, 19.8, 29.7, 39.8, 49.5	3.47
Slice thickness (mm)	4	4	4
In-plane resolution (mm)	1.1	1.1	1.1
Slice gap (mm)	0	0	0
Flip angle (°)	4, 21	N/A	7
Number of slices	20	20	20
Preparation pulse	–	–	MTC pulse on, off

MTR magnetization transfer ratio, *FLASH* fast low-angle shot gradient echo, *MTC* magnetization transfer contrast

Image acquisition and assessment for adjusted-SETI TSE

Two-slice TSE images were obtained and evaluated by adjusting the SETI in multiple steps (i.e., adjusted-SETI TSE) to assess how the differences in the SETI affect the observed signal intensity due to the MT effect (Fig. 2). The electrocardiogram (ECG) synchronization function (ESF) and pseudoelectrocardiogram (pseudo-ECG) wave generation function (pECGF) equipped in the MR device were used to adjust the SETI. The pECGF can mechanically generate pseudo-ECG pulses at arbitrary intervals that can be passed to the ESF as a trigger to start a scan. Thus, the SETI could be adjusted using these functions. In addition, the TR was changed in three steps (400, 1000, and 3000 ms) because the length of the TR generally affects the MT-effect-induced change in the signal [17]. The SETIs

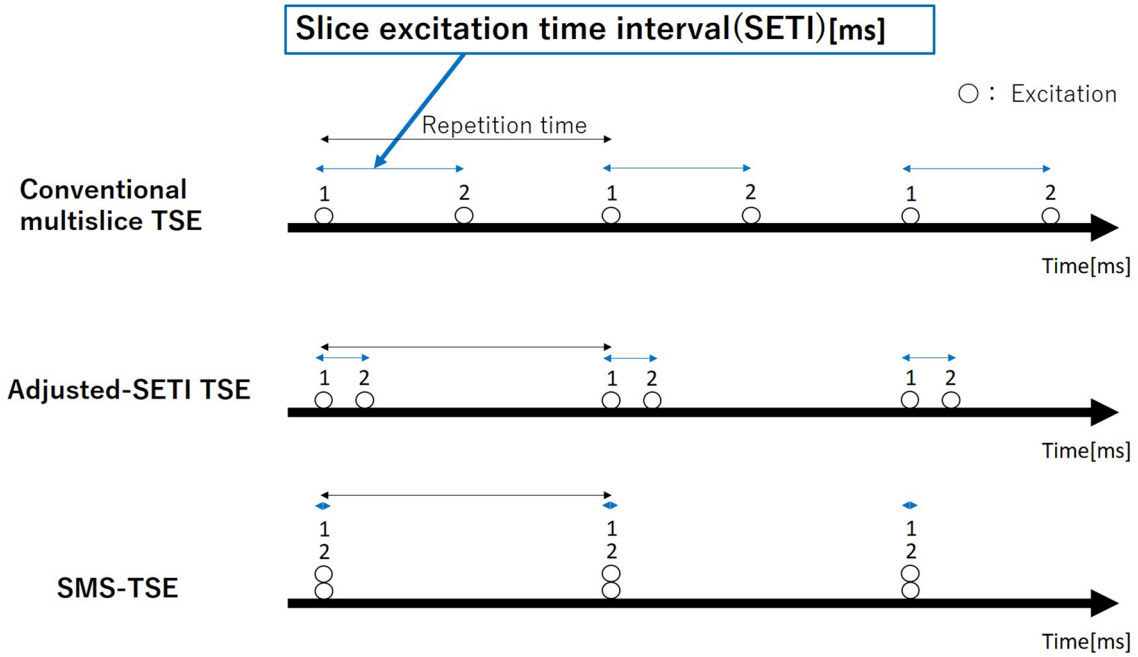

Fig. 2 The time interval between the scans of two different slices was assessed as a factor to alter the magnetization transfer (MT)-effect-related reduction in the signal. The circles with numbers indicate the excitation times for the first and second slices. The excitation of the first slice generates the magnetization of macromolecular protons, and the second slice is where the reduction in the signal due to the MT effect will be observed. Conventional multislice turbo spin echo (TSE) images were acquired by changing the slice excitation time interval (SETI) in multiple steps (adjusted-SETI turbo spin echo: adjusted-SETI TSE) to evaluate the effect of the SETI on the MT-effect-related reduction in the signal. Images of a simultaneous multislice turbo spin echo (SMS-TSE) sequence, which simultaneously excites two slices, were also acquired to compare them with images of adjusted-SETI TSE

were 50, 150, and 200 ms for TR = 400 ms; 50, 100, 200, 300, 400, and 500 ms for TR = 1000 ms; and 50, 100, 200, 300, 400, 500, 600, 700, 800, 900, 1000, 1100, 1200, 1300, 1400, and 1500 ms for TR = 3000 ms. The other imaging parameters were fixed at TE = 9.3 ms, number of slices = 2, slice thickness = 4 mm, in-plane resolution = 1.1 mm, and echo train length (ETL) = 4. In addition, to observe the exact MT-effect-related change in the signal without the effect of interslice crosstalk due to the incompleteness of the slice profile, the slice gap for imaging was set to 8 mm, which was twice the width of the applied slice thickness. The signal intensities were measured and averaged on the basis of the ROIs of the second-slice image of each adjusted-SETI TSE acquisition (where the change in the signal due to the MT effect would be observed). The averaged signal intensities of the phantoms were normalized by the signal intensity of the ultrapure water phantom so that the average values from either different SETIs or TRs would be directly comparable. The ultrapure water phantom was suitable for this purpose because there is no MT effect in this phantom. For each TR in each phantom, the signal intensities at different SETIs were plotted to observe the relation between the SETI and the acquired signal intensity. This relation was further assessed by a Pearson's correlation analysis, and $P < 0.05$ was considered significant. Here, the ratio of the decrease in the signal related to the SETI (rsdSETI) was defined as an index that reflects how much the difference in the SETI affects the signal intensity in each phantom and the TR:

$$(A, B) = \arg\min_{a,b} \sum_{i}^{N} \left[S_i - \left(a\mathrm{SETI}_i + b\right)\right]^2, \tag{2}$$

$$\mathrm{rsdSETI} = A, \tag{3}$$

where SETI_i is the specific SETI length, S_i is the observed signal intensity at SETI_i, and N is the number of different SETIs applied for each phantom and each TR. Thus, A (which equals rsdSETI) and B correspond to the slope and intercept of the line that approximates the signal intensity for each TR and each phantom using the least-squares method. Then, the obtained values of rsdSETI were compared among different TRs and phantoms.

Image acquisition and assessment for SMS-TSE

This section aims to compare the SMS-TSE images with the adjusted-SETI TSE images discussed in the previous section. Images were acquired by SMS-TSE after images were acquired by adjusted-SETI TSE; thus, the scanned slices will

be consistent for all acquisitions. Images were acquired by SMS-TSE by simultaneously exciting the two slices using a multiband technique. The slice gap was 8 mm, and the TR was set to 400, 1000, and 3000 ms—the same as that in adjusted-SETI TSE. Moreover, the other major parameters [e.g., the TE, number of slices, slice thickness, field of view (FOV), matrix size, and ETL] were also set to the same values used for adjusted-SETI TSE. The representative signal intensities for evaluation were measured and averaged on the basis of the ROIs. Then, these values were normalized in the same manner as done for adjusted-SETI TSE. The signal intensity of SMS-TSE for each phantom and TR was compared with the signal intensity of the corresponding adjusted-SETI TSE. Furthermore, the following assessment was performed to evaluate whether the signal intensity of SMS-TSE was similar to the assumed signal intensity of adjusted-SETI TSE at SETI = 0 ms, despite the differences between these imaging sequences. First, the root-square error (RSE) between the measured adjusted-SETI TSE signal intensity and the fitted line obtained in the previous section were calculated as

$$\mathrm{RSE}_i = \left[\left(S_i - A \cdot \mathrm{SETI}_i - B\right)^2\right]^{\frac{1}{2}}, \tag{4}$$

where RSE_i is the RSE for SETI_i, S_i is the measured signal intensity at SETI_i. and A and B are the constants obtained using Eq. 2. Then, their mean value (root-mean-square error: RMSE) was also calculated for each TR and each phantom as

$$\mathrm{RMSE} = \frac{1}{N}\sum_{i}^{N} \mathrm{RSE}_i, \tag{5}$$

where N is the number of different SETIs applied for each setting.

In addition, the RSE for SMS-TSE ($\mathrm{RSE}_{\mathrm{SMS}}$) was calculated for each TR and each phantom by comparing the signal intensity of SMS-TSE with the linear approximation for the corresponding adjusted-SETI TSE as

$$\mathrm{RSE}_{\mathrm{SMS}} = \left[\left(S_{\mathrm{SMS}} - B\right)^2\right]^{\frac{1}{2}}, \tag{6}$$

where S_{SMS} is the signal intensity of SMS-TSE. Note that A in Eq. 4 does not appear in Eq. 6 because the SETI for SMS-TSE was considered to be zero. A measured signal intensity belonging to either adjusted-SETI TSE or SMS-TSE was defined as an outlier when its corresponding RSE_i or $\mathrm{RSE}_{\mathrm{SMS}}$ was larger than three times the RMSE. An assessment was performed to determine whether the signal intensity of SMS-TSE would become the only outlier among all of the signal intensities of adjusted-SETI TSE and SMS-TSE.

Additional assessment for human brains

This additional section aims to briefly explore the reproducibility of the phantom results in a human-based study.

Brains of four healthy volunteers (male 27–37 years old) with no particular past history were scanned with the same MRI scanner as that used for the phantoms. The whole imaging protocol included adjusted-SETI TSE scans and an SMS-TSE scan in TR 400 ms. Two pseudo-spoiler pulses were added to each of these acquisitions to remove the effect of residual transverse magnetization due to the flow and inhomogeneity in an in vivo brain tissue. The other imaging parameters were kept identical with the phantom scans, except that SETI at 50 ms was not applied for adjusted-SETI TSE in this scan as it was unavailable due to the additional pseudo-spoiler pulses. Therefore, the adjusted-SETI TSE scans included SETI = 100, 150, and 200 ms. The slice at the basal ganglia level was selected for each image series in each volunteer. Three ROIs were set on the images located at the putamen area, the deep white matter area around the superior longitudinal fasciculus, and the deep white matter area around the occipital lobe (Fig. 3). The latter two areas

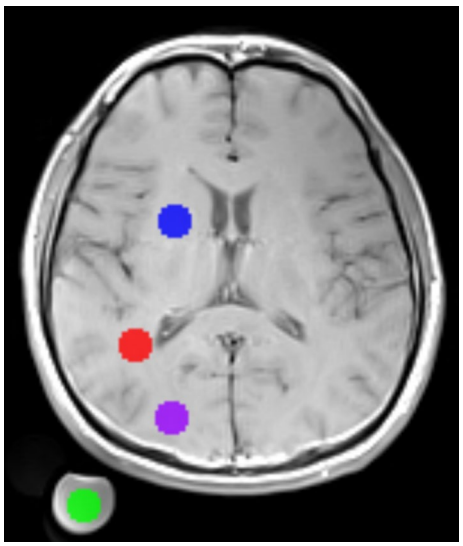

Fig. 3 Signal intensities of adjusted slice excitation time interval turbo spin echo (adjusted-SETI TSE) and simultaneous multislice turbo spin echo (SMS-TSE) were additionally evaluated for four human brains using a region of interest (ROI) based study. The slice at the basal ganglia level was selected from each volunteer, and then, three ROIs were manually designed. The ROIs were located at the putamen area (blue), the area around the superior longitudinal fasciculus (red), and the area around the deep occipital white matter (purple). The signal intensities of the pixels included in each ROI were averaged to obtain a representative value for the ROI, and then they were normalized by the signal intensity of the pure water phantom scanned in the same slice (green). Furthermore, the normalized signal intensities for each ROI were averaged between the volunteers (color figure online)

were selected because these areas had the most spacious and homogeneous white matter area at the selected slice level. Signal intensities of the pixels within each ROI were averaged, and then they were normalized using a simultaneously scanned pure water phantom, similar to the phantom study (Fig. 3). The normalized signals were further averaged between the four volunteers, and then the relation between the signal intensities and SETI length was assessed.

Results

Evaluation of the phantoms

Table 2 summarizes the measured values of *T*1, *T*2, and the MTR for each phantom. The values from previous reports [11, 12] are also indicated in parentheses as a reference. The measured values were in good agreement with the reference values. Comparing the values between different agar concentrations, *T*1 and *T*2 were lower, and the MTR was higher for a phantom with a higher agar concentration.

Evaluation of the signal intensities of adjusted-SETI TSE

For all combinations of TRs and phantoms, a shorter SETI resulted in a lower signal intensity (Fig. 4). The values for Pearson's correlation coefficient between the SETI and the signal intensity for each TR and each phantom are listed in Table 3. Strong correlations ($R > 0.8$) were observed, except for the phantom with an agar concentration of 2% at TR = 400 and 1000 ms; in particular, the correlations were

Table 2 *T*1, *T*2, and magnetization transfer ratios of the phantoms

	Ultrapure water	Agar concentration		
		2%	4%	8%
*T*1 (ms)	3137	2612 (2514–3060)	2189 (2400–2405)	1550 (1690–1973)
*T*2 (ms)	1442	91 (54–80)	42 (29–37)	16 (12–17)
MTR	0.01	0.20 (0.19)	0.33 (0.31)	0.45 (0.47)

The numbers in the parentheses indicates the reference values cited from previously published reports

MTR magnetization transfer ratio

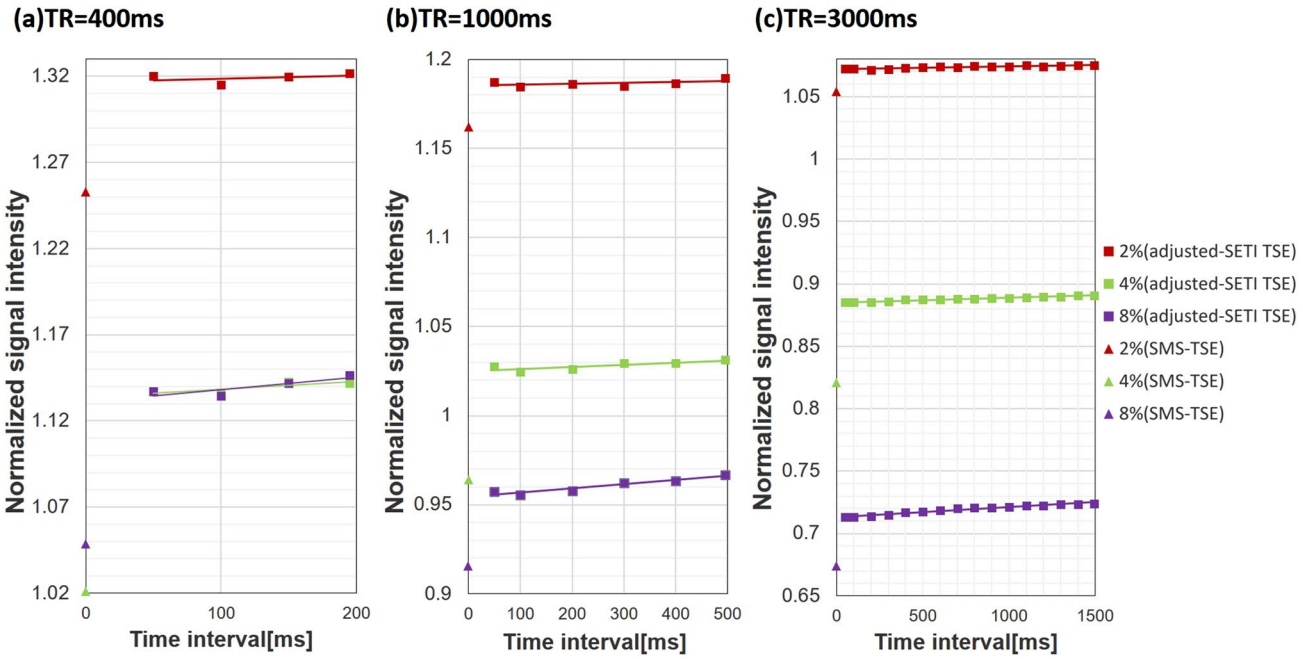

Fig. 4 The observed signal intensities of adjusted slice excitation time interval (SETI) turbo spin echo (TSE) (adjusted-SETI TSE) and simultaneous multislice TSE (SMS-TSE) in the phantom study. The signals were normalized by the signal of the ultrapure water phantom at each TR. The lines are the linear approximations for the corresponding adjusted-SETI TSE plots. A shorter SETI resulted in a lower signal intensity for adjusted-SETI TSE for all combinations of repetition times and agar concentrations. The signal intensities of SMS-TSE were always lower than the corresponding adjusted-SETI TSE signal intensities

Table 3 Result of Pearson's correlation analysis between the SETI and the signal intensity

Agar concentration (%)	Repetition time (ms)		
	400	1000	3000
2	0.424 (0.544)	0.530 (0.258)	0.894 (0.000)
4	0.859 (0.076)	0.833 (0.024)	0.982 (0.000)
8	0.859 (0.076)	0.955 (0.001)	0.980 (0.000)

The numbers indicate Pearson's correlation coefficients (R). The values in the parentheses are the P values. $P < 0.05$ was considered as a significant correlation

SETI slice excitation time interval

significant for phantoms with an agar concentration of 2% with a TR of 3000 ms, an agar concentration of 4% with TRs of 1000 and 3000 ms, and an agar concentration of 8% with TRs of 1000 and 3000 ms ($P < 0.05$). In every case, the rsdSETI was positive (Fig. 5). In addition, the rsdSETI was higher for phantoms with a higher agar concentration for each TR and higher at a shorter TR for each phantom (Fig. 5).

Evaluation of the signal intensities of SMS-TSE

For all combinations of the TRs and phantoms, the signal intensity of SMS-TSE was smaller than that of adjusted-SETI TSE (Fig. 4). The RSEs for the differences between the signal intensity of adjusted-SETI TSE and the linear approximation were relatively small and converged to a narrow range without any outliers for each TR and each phantom. On the other hand, RSE_{SMS} for each TR and each phantom was relatively large compared to the RSEs of adjusted-SETI TSE, and all of them were in the range of the outliers (Fig. 6).

Evaluation of the signal intensities of human brain

The averaged signal intensity of adjusted-SETI TSE monotonically decreased as the SETI length decreased in all the ROIs (Fig. 7). In addition, the signal intensity of SMS-TSE was always smaller than the signal intensities of adjusted-SETI TSE (Fig. 7). These results were similar to those of the phantom studies.

Discussion

To prepare multiple phantoms with different MTRs, three types of agar phantoms with different concentrations were created in this study. In these phantoms, the $T1$ and $T2$ values were smaller, and the MTR was larger in phantoms with a higher agar concentration. The differences in the $T1$ and $T2$ values are due to the smaller $T1$ and $T2$ values of agar compared to those of pure water [11, 12, 21]. In addition, the MTR was larger for a phantom with a higher agar concentration because the number of agar macromolecules that can contribute to the MT effect increases at a higher agar concentration [18]. The measured $T1$, $T2$, and the MTR values of the agar phantoms were similar to those in previous reports [19, 22, 23]; therefore, we considered that it is reasonable to use these phantoms for this study. On the other hand, it was desirable to maintain identical $T1$ and $T2$ values for phantoms with different agar concentrations because $T1$ and $T2$ affect the MT effect in addition to MTR. However, it was not achieved in this study owing to a technical difficulty.

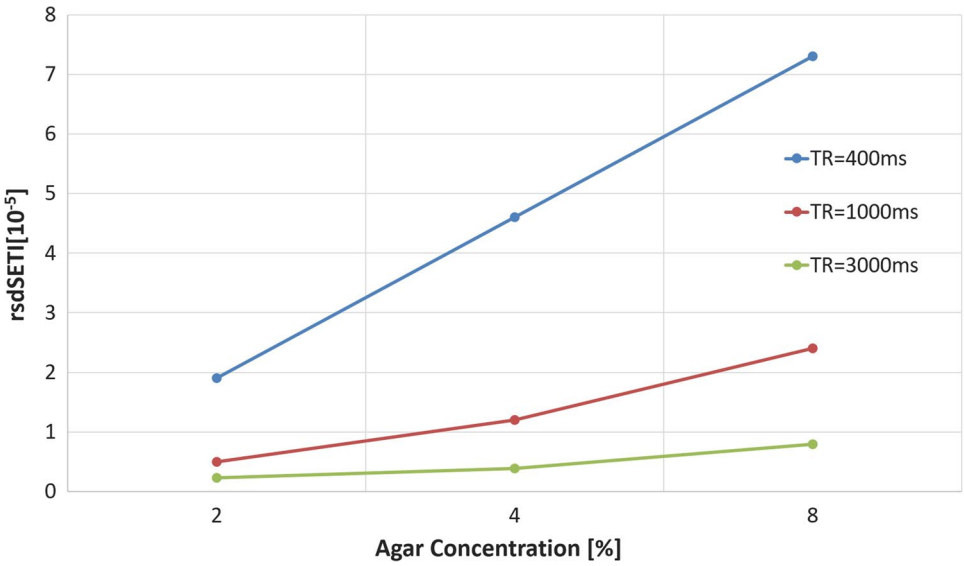

Fig. 5 The ratio of the signal decrease related to the slice excitation time interval (SETI) (rsdSETI) obtained for the phantom study. The rsdSETI corresponds to the slope of the line that approximates the signal intensities of adjusted-SETI turbo spin echo (TSE) (see the lines in Fig. 4), which reflect how strongly the change in the SETI affects the signal intensity in each setting. As shown, the rsdSETI was relatively larger when the agar concentration was higher and the repetition time was shorter

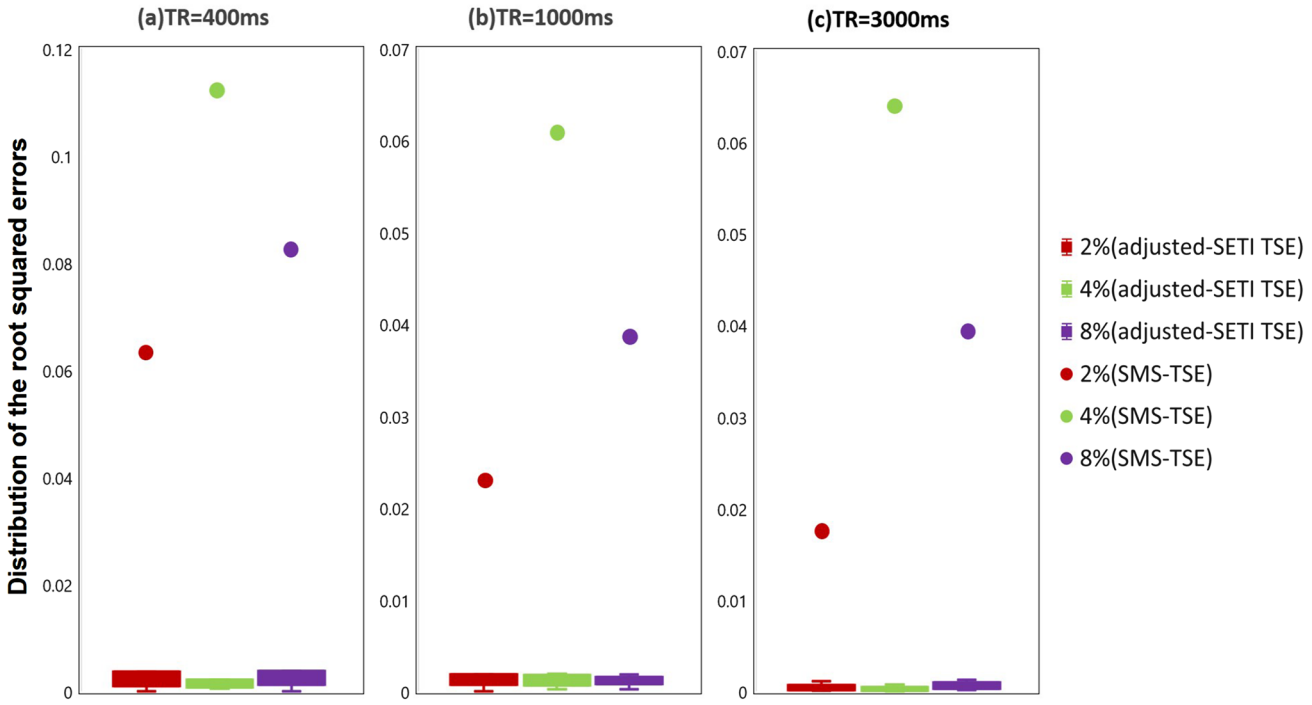

Fig. 6 Distributions of the root-squared errors (RSE) of the adjusted slice excitation time interval (SETI) turbo spin echo (TSE) (adjusted-SETI TSE) and simultaneous multislice TSE (SMS-TSE) signals compared to the linearly approximated lines obtained for the adjusted-SETI TSE signals (phantom study). The linear approximations are the same as those shown in Fig. 4 [the slopes of these lines were defined as the rsdSETI (Fig. 5)]. The boxplot and dot at each repetition time and agar concentration indicate the distribution of the RSEs for the adjusted-SETI TSE signals and the RSE for the SMS-TSE signals, respectively. The RSEs were relatively small and distributed in a narrow range for adjusted-SETI TSE. However, the RSEs were relatively large for SMS-TSE and beyond the level of an outlier in all settings [the values were larger than three times the root-mean-square error (RMSE; not shown)]

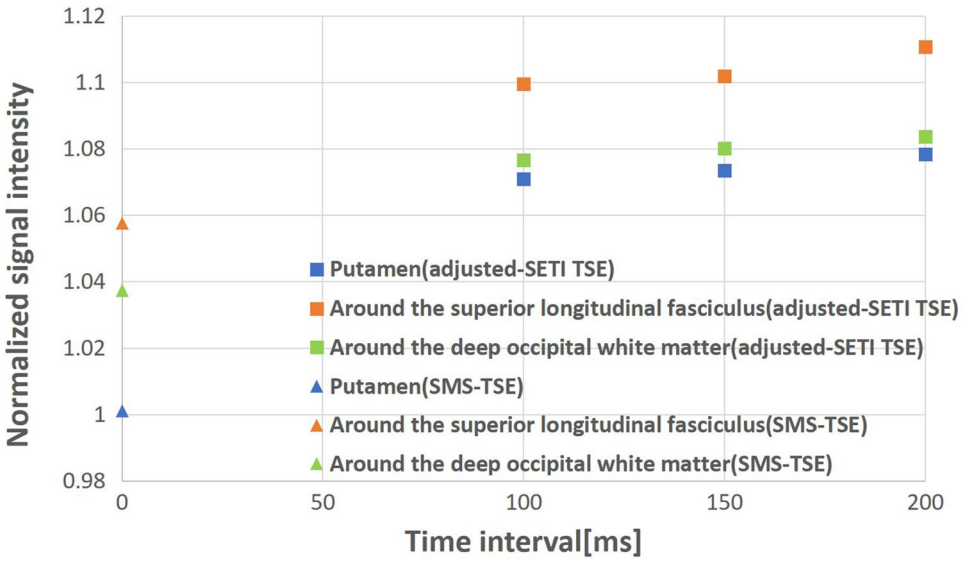

Fig. 7 Normalized and averaged signal intensities of adjusted slice excitation time interval (SETI) turbo spin echo (TSE) (adjusted-SETI TSE) and simultaneous multislice TSE (SMS-TSE) in human brain. Signal intensities of adjusted-SETI TSE decreased as SETI became shorter. The signal intensity of SMS-TSE was even smaller than adjusted-SETI TSE signals, similar to the result of the phantom study (see Fig. 4)

From the assessments of adjusted-SETI TSE, the strength of the influence of the SETI on the MT effect was evaluated. As indicated by the results, the signal reduction was smaller when the SETI was longer (Fig. 4). This result can be explained as follows. The liquid protons partially saturated by the MT pulse gradually relax longitudinally within the SETI. Thus, the number of partially saturated protons at the time of excitation of the second slice will be lower when

the SETI is long, which means that a longer SETI results in a smaller reduction in the signal due to the MT effect.

From the correlation analysis performed to confirm the relationship between the SETI and the signal intensity, high linear correlation coefficients of $R > 0.8$ were observed for most TR and phantom combinations. In particular, a significant correlation was observed for phantoms with an agar concentration of 2% and TR = 3000 ms, an agar concentration of 4% and TR = 1000 and 3000 ms, and an agar concentration of 8% and TR = 1000 and 3000 ms. These results suggest the validity of the linear approximation between the SETI and the signal intensity of adjusted-SETI TSE within the ranges of parameter values used in this study. The correlation coefficients for phantoms with an agar concentration of 2% and TR = 400 and 1000 ms were small, most likely because the change in the signal intensity related to the MT effect was too small owing to the very low agar concentration.

The rsdSETI reflects the magnitude of the influence of the SETI on the degree of signal reduction in each specific setting (Fig. 5). Note that this value is the slope when the relation between the SETI and the measured signal intensities was linearly approximated by the least-squares method. This linear approximation is based on the validity of the significant linear correlation between the SETI and the signal intensity from the Pearson's correlation analysis. From the results of this study, the rsdSETI was larger when the agar concentration was higher for the same TR and when the TR was shorter for the same agar concentration (Fig. 5). The results show that the influence of the SETI was stronger under conditions where the MT effect generally appears stronger.

In addition to the MT effect, the influence of crosstalk between the slices due to incompleteness of the slice profile can potentially affect the observed signal intensity [24]. However, the slice gap set to 200% of the slice thickness (4 mm) in this study might be enough to avoid this effect [see supplementary experiment (Online Resource 1) for additional discussion].

The signal intensity of SMS-TSE was lower than that of adjusted-SETI TSE in all the settings (Fig. 4). In addition, the signal reduction of SMS-TSE was very large compared to that of adjusted-SETI TSE. As shown in Fig. 4, the signal intensities of adjusted-SETI TSE are close to the linear approximations with very low errors, but the signal intensities of SMS-TSE were far below these lines. The deviations from these lines were further assessed by comparing the RSEs (Fig. 6). RSE_{SMS} was much larger than the RSEs of adjusted-SETI TSE, which by far exceeded the level distinguished as an outlier. This means that the reason why the MT effect of SMS-TSE is the strongest cannot be explained solely by the shortest scan time interval between the two slices.

As one possible reason for explaining the large MT effect in SMS-TSE, the relation between the SETI and the signal intensity might be different in a smaller SETI range because the MT effect might be nonlinear if the difference in the SETI mainly reflects the level of longitudinal relaxation of saturated protons. This question can be answered by adding scans with shorter SETIs. However, it was not available in this study because ETL for the scans was fixed to four to observe the MT effect sufficiently. The SETI can be shortened if the ETL is smaller, but the MT effect also becomes small [25, 26].

As another possible reason, the RF pulse is not the same for conventional TSE and SMS-TSE. In SMS-TSE, the energy magnitude of an RF pulse is relatively large compared to that of conventional TSE because multiple slices are simultaneously excited. Therefore, the limitations related to the specific absorption ratio (SAR) and the maximum applied voltage of the RF power amplifier become problematic in SMS-TSE. To overcome these problems, SMS-TSE adopts a variable-rate selective excitation (VERSE)-waveform RF pulse instead of the sinc-waveform RF pulse used in conventional TSE. The VERSE-waveform RF pulse for SMS-TSE is designed so that the number of excited protons and the flip angle become the same as those obtained with the sinc-waveform RF pulse. However, the VERSE-waveform RF pulse gradually alters the magnetic gradient strength during a scan. This means that other important parameters, including the offset frequency, bandwidth, and RF duration, might not be consistent during excitation. These differences in the RF pulse may also be a reason for the strong MT effect found in SMS-TSE. Additional multi-slice scan using VERSE-waveform RF pulse and adjusted-SETI may help further understand this problem; however, such a scan was not available in the work-in-progress imaging sequence used in this study. For the same reason, other additional evaluations of the VERSE-waveform RF pulse (e.g., visualizing the slice profile) were also not available.

Scans for human brain were additionally performed to verify the reproducibility of the results seen in the phantom studies. The scan design was simplified to accomplish the whole scan within a reasonable scan time. The parameters were selected so that the settings would be practical considering the clinical *T*1-weighted image scans.

The relation between the SETI length and signal intensity of adjusted-SETI TSE in human subjects was similar to that found in the phantom study, where the signal was lower in shorter SETI in all the ROIs (Fig. 7). In addition, the characteristic of the signal reduction of SMS-TSE being larger than the level of supposedly linear decrease of adjusted-SETI TSE was also similar to the phantom study (Fig. 7). Thus, we may imply that the results of the phantom study were well reproduced in humans at least within the examined range.

In this study, it was shown that the MT effect appears strongly in the SMS-TSE imaging compared to the conventional multislice TSE imaging. This characteristic should carefully be mentioned in clinical settings because the image contrast might be more greatly affected by the MT effect. However, there is a possibility that more useful imaging can be performed by effectively using this characteristic. As examples, Gd-enhanced imaging [27] and neuromelanin imaging [28, 29] using SMS-TSE may achieve a higher contrast than that obtained with the conventional TSE. Moreover, the acquisition time would be relatively shorter, which may be desirable for clinical scans.

There are several limitations in this study. Most of all, the RF pulses applied for adjusted-SETI TSE and that applied for SMS-TSE were different, as mentioned above. This limitation was unable to overcome due to a technical reason. Therefore, the reason for the strong MT effect of SMS-TSE was not thoroughly evaluated. An additional study is necessary to prove supplement this problem. The other limitations are as follows. First, the *T*1 and *T*2 values of the phantoms were not identical. The addition of a material such as manganese may help to overcome this problem, but it was not performed in this study owing to a technical difficulty. Second, the SETI could not be set to less than 50 ms because the ETL was fixed at four to ensure that the MT effect was sufficiently large. Third, the effect of the differences in the RF pulses of conventional TSE and SMS-TSE was not isolated for discussion in this study owing to a technical difficulty.

In conclusion, shorter SETI results in a larger MT effect in conventional multislice TSE. The contrast change in SMS-TSE was even larger than the level supposable from its simultaneous excitation, which needs to be considered in clinical use.

Acknowledgements The authors would like to thank Hiroshi Koide, Ph.D. and Ms. Tomomi Ikeda of the Laboratory of Molecular and Biochemical Research, Research Support Center, Juntendo University, Graduate School of Medicine for their cooperation to create a phantom.

Funding This work was supported in part by the ImPACT Program of the Council for Science, Technology and Innovation (Cabinet Office, Government of Japan) and by a Grant-in-Aid for Scientific Research on Innovative Areas (ABiS) from the Ministry of Education, Culture, Sports, Science and Technology of Japan and by JSPS KAKENHI (Grant number 18H02772).

Compliance with ethical standards

Conflict of interest Katsutoshi Murata is an employee of Siemens Healthcare K.K., Japan. All remaining authors declare no conflicts of interest associated with this manuscript.

Ethical statement This study was approved by the local ethics review board of Juntendo University and subjects informed consent were obtained.

References

1. Feinberg DA, Setsompop K. Ultra-fast MRI of the human brain with simultaneous multi-slice imaging. J Magn Reson. 2013. https://doi.org/10.1016/j.jmr.2013.02.002.
2. Setsompop K, Cohen-Adad J, Gagoski BA, Raij T, Yendiki A, Keil B, et al. Improving diffusion MRI using simultaneous multi-slice echo planar imaging. NeuroImage. 2012. https://doi.org/10.1016/j.neuroimage.20106.033.
3. Takamura T, Hori M, Kamagata K, Kumamaru KK, Irie R, Hagiwara A, et al. Slice-accelerated gradient-echo echo planar imaging dynamic susceptibility contrast-enhanced MRI with blipped CAIPI: effect of increasing temporal resolution. Jpn J Radiol. 2018. https://doi.org/10.1007/s11604-017-0695-y.
4. Benali S, Johnston PR, Gholipour A, Dugan ME, Heberlein K, Bhat H, et al. Simultaneous multi-slice accelerated turbo spin echo of the knee in pediatric patients. Skelet Radiol. 2018. https://doi.org/10.1007/s00256-017-2868-2.
5. Fritz J, Fritz B, Zhang J, Thawait GK, Joshi DH, Pan L, et al. Simultaneous multislice accelerated turbo spin echo magnetic resonance imaging: Comparison and combination with in-plane parallel imaging acceleration for high-resolution magnetic resonance imaging of the knee. Investig Radiol. 2017. https://doi.org/10.1097/rli.0000000000000376.
6. Clare M, Mark Henkelman R. A model for magnetization transfer in tissues. Magn Reson Med. 1995. https://doi.org/10.1002/mrm.1910330404.
7. Morrison C, Stanisz G, Henkelman RM. Modeling magnetization transfer for biological-like systems using a semi-solid pool with a super-lorentzian lineshape and dipolar reservoir. J Magn Reson B. 1995. https://doi.org/10.1006/jmrb.1995.1111.
8. Caines GH, Schleich T, Rydzewski JM. Incorporation of magnetization transfer into the formalism for rotating-frame spin-lattice proton NMR relaxation in the presence of an off-resonance-irradiation field. J Magn Reson (1969). 1991. https://doi.org/10.1016/0022-2364(91)90169-T.
9. Wu X. Lineshape of magnetization transfer via cross relaxation. J Magn Reson (1969). 1991. https://doi.org/10.1016/0022-2364(91)90308-G.
10. Hoffman RA, Forsén S. Transient and steady-state overhauser experiments in the investigation of relaxation processes. Analogies between chemical exchange and relaxation. J Chem Phys. 1966. https://doi.org/10.1063/1.1727890.
11. Martirosian P, Boss A, Deimling M, Kiefer B, Schraml C, Schwenzer NF, et al. Systematic variation of off-resonance prepulses for clinical magnetization transfer contrast imaging at 0.2, 1.5, and 3.0 Tesla. Investig Radiol. 2008. https://doi.org/10.1097/RLI.0b013e3181559949.
12. Fabian S, Petros M, Jürgen M, Schwenzer NF, Claussen CD, Fritz S. Magnetization transfer contrast imaging in bovine and human cortical bone applying an ultrashort echo time sequence at 3 Tesla. Magn Reson Med. 2009. https://doi.org/10.1002/mrm.21866.
13. Wolff SD, Balaban RS. Magnetization transfer contrast (MTC) and tissue water proton relaxation in vivo. Magn Reson Med. 1989. https://doi.org/10.1002/mrm.19101001.
14. Wolff SD, Chesnick S, Frank JA, Lim KO, Balaban RS. Magnetization transfer contrast: MR imaging of the knee. Radiology. 1991. https://doi.org/10.1148/radiology.179.3.2027963.
15. Chang Y, Bae SJ, Lee YJ, Hwang MJ, Lee SH, Lee J, et al. Incidental magnetization transfer effects in multislice brain MRI at 3.0T. J Magn Reson Imaging. 2007. https://doi.org/10.1002/jmri.20867.

16. Santyr GE. Magnetization transfer effects in multislice MR imaging. Magn Reson Imaging. 1993. https://doi.org/10.1016/0730-725X(93)90471-O.
17. Henkelman RM, Stanisz GJ, Graham SJ. Magnetization transfer in MRI: a review. NMR Biomed. 2001. https://doi.org/10.1002/nbm.683.
18. Henkelman RM, Huang X, Xiang QS, Stanisz GJ, Swanson SD, Bronskill MJ. Quantitative interpretation of magnetization transfer. Magn Reson Med. 1993. https://doi.org/10.1002/mrm.1910290607.
19. Belton PS, Hills BP, Raimbaud ER. The effects of morphology and exchange on proton N.M.R. relaxation in agarose gels. Mol Phys. 1988. https://doi.org/10.1080/00268978800100591.
20. Chung S, Kim D, Breton E, Axel L. Rapid B1+ mapping using a preconditioning RF pulse with TurboFLASH readout. Magn Reson Med. 2010. https://doi.org/10.1002/mrm.22423.
21. Hellerbach A, Schuster V, Jansen A, Sommer J. MRI phantoms—are there alternatives to agar? PLoS ONE. 2013. https://doi.org/10.1371/journal.pone.0070343.
22. Sled JG, Bruce PG. Quantitative imaging of magnetization transfer exchange and relaxation properties in vivo using MRI. Magn Reson Med. 2001. https://doi.org/10.1002/mrm.1278.
23. Sled JG, Pike GB. Quantitative interpretation of magnetization transfer in spoiled gradient echo MRI sequences. J Magn Reson. 2000. https://doi.org/10.1006/jmre.2000.2059.
24. Zhuo J, Gullapalli RP. MR artifacts, safety, and quality control. RadioGraphics. 2006. https://doi.org/10.1148/rg.261055134.
25. Constable RT, Anderson AW, Zhong J, Gore JC. Factors influencing contrast in fast spin-echo MR imaging. Magn Reson Imaging. 1992. https://doi.org/10.1016/0730-725X(92)90001-G.
26. Matthias W, Gunther H, Juergen H. Investigation and modeling of magnetization transfer effects in two-dimensional multislice turbo spin echo sequences with low constant or variable flip angles at 3 T. Magn Reson Med. 2010. https://doi.org/10.1002/mrm.22145.
27. Elster AD, King JC, Mathews VP, Hamilton CA. Cranial tissues—appearance at gadolinium-enhanced and nonenhanced MR-imaging with magnetization-transfer contrast. Radiology. 1994. https://doi.org/10.1148/radiology.190.2.8284413.
28. Nakane T, Nihashi T, Kawai H, Naganawa S. Visualization of neuromelanin in the substantia nigra and locus ceruleus at 1.5T using a 3D-gradient echo sequence with magnetization transfer contrast. Magn Reson Med Sci. 2008. https://doi.org/10.2463/mrms.7.205.
29. Wolff SD, Balaban RS. Magnetization transfer imaging: practical aspects and clinical applications. Radiology. 1994. https://doi.org/10.1148/radiology.192.3.8058919.